Available online at www.sciencedirect.com
ScienceDirect
Journal of Sound and Vibration 309 (2008) 407–425
JOURNAL OF SOUND AND VIBRATION
www.elsevier.com/locate/jsvi

Vehicle–bridge interaction analysis under high-speed trains

Nan Zhang*, He Xia, Weiwei Guo

School of Civil Engineering & Architecture, Beijing Jiaotong University, Beijing 100044, China

Received 13 July 2006; received in revised form 3 July 2007; accepted 11 July 2007
Available online 27 September 2007

Abstract

The dynamic interaction between high-speed train and simply supported girders is studied by theoretical analysis and field experiment in this paper. The dynamic interaction model of the train–bridge system is established, in which the rigid-body dynamics theory, finite element method and wheel–rail displacement corresponding assumption are adopted for the vehicle model, bridge model and wheel–rail interaction model, respectively. The measured track irregularities are taken as the system excitation. The responses of a 24 m-span PC box girder bridge are calculated. The proposed analysis model and the solution method are verified through the comparison between the calculated results and the measured results.

1. Introduction

The impact effect of the train plays an important role in railway bridge design. As proved in former studies, the dynamic responses of bridges and vehicles increase with the running speed and the axle load of the train [1–3,6–9,11]. With the development of high-speed and heavy-load railways, it is inevitable to take the dynamic factors into account in predicting the internal force and deflection status of bridge structures under running trains, to ensure the serviceability of the bridge and the running safety and stability of the train vehicles.

The Qinhuangdao-Shenyang Special Passenger Railway (QSSPR) is the first high-speed railway in China, which was completed in 2002 and put into operation in 2003. The design train speed is 300 km/h for the General Experimental Section of QSSPR and 200 km/h for the rest of the railway. In order to study the safety and reliability of bridges under high-speed trains, the dynamic properties of all types of girders adopted in the General Experimental Section of QSSPR, including single-bound and double-bound simply supported box girders, double-bound simply supported T-section girders and double-bound continuous I-section composite girders, were checked by the vehicle–bridge interaction analysis in the design phase and proved safety under high-speed trains by the field experiments.

The research on vehicle–bridge interactions developed greatly in recent decades, which was mainly focused on the following problems: modeling of vehicle, modeling of bridge, modeling of wheel–rail interaction, adoption of track irregularities and numerical solution algorithms for vehicle–bridge interaction equations. All these problems are discussed in Section 2 of this paper.

*Corresponding author. Tel.: +86 10 51683786; fax: +86 10 51683340.
E-mail address: nanzhang@263.net (N. Zhang).

0022-460X/$ - see front matter © 2007 Elsevier Ltd. All rights reserved.
doi:10.1016/j.jsv.2007.07.064

In the paper, a dynamic model for simulating the movement of vehicle–bridge interaction system is established and the corresponding computer code is worked out. The dynamic responses of the Gouhe River Bridge, a bridge consisting of 28-span 24 m double-bound simple-supported box girders, under the Pioneer Train, are studied by both field experiment and calculation.

2. Dynamic model of vehicle–bridge interaction system

The dynamic model for the vehicle–bridge interaction system is composed of a train subsystem and a bridge subsystem. The two subsystems are linked by the assumed wheel–rail interactions. The track irregularity and the numerical integral method are also discussed for the vehicle–bridge interaction system.

2.1. Train subsystem model

The train subsystem (also called vehicle subsystem) model, as those used in most researches [1,4,5,10,13,14,19,20], adopts the following assumptions:

(1) The train runs on the bridge at a constant speed.
(2) Except for some kinds of articulated trains [4,5], the train can be modeled as several independent vehicle elements. Each vehicle element is composed of a car body, two bogies, four or six wheel-sets and the spring-damping suspensions between the components.
(3) The car body, bogies and wheel-sets in each vehicle element are regarded as rigid components, neglecting their elastic deformation in vibration.
(4) The connections between a bogie and its wheel-sets are characterized by the first suspension system, which consists of springs and dampers with identical properties. A lateral spring, a vertical spring, a lateral damper and a vertical damper are assumed at each side of a wheel-set.
(5) The connections between a car body and its bogies are characterized by the second suspension system, which consists of springs and dampers with identical properties. A lateral spring, a vertical spring, a lateral damper and a vertical damper are assumed at each side of a bogie.
(6) The springs in vehicle elements are all with linear property, and the dampers all with viscous property.
(7) Each car body or bogie has 5 dofs (degree of freedom) in directions of Y, Z, R_X, R_Y and R_Z, while the movement in direction X, namely the longitudinal movement, is neglected.

The main difference among the vehicle models in different researches is the selection of dof for the wheel-set, which relates to the wheel–rail interaction model adopted, as discussed in Section 2.3. In this analysis, three dofs in Y, Z and R_X directions for a wheel-set are selected, thus each vehicle element has 27 dofs for a 4-axle vehicle and 33 dofs for a 6-axle one. The vehicle model for a 4-axle vehicle is shown in Fig. 1.

In the figure, subscripts 1, 2 and 3 in each dof denote the car body, the front bogie and the rear bogie, subscripts 4 and 5 denote the first and the second wheel-sets at the front bogie, and subscripts 6 and 7 denote the first and the second wheel-sets at the rear bogie, respectively. In the wheel–rail interaction model, the dofs of the wheel-sets are regarded as the links between the vehicle subsystem and the bridge subsystem, thus they are not independent in either of the two subsystems. By assuming small vibration amplitude of each component in a vehicle element, the equations of motion for the car body and two bogies in a vehicle element can be expressed as

$$[M_V]\{\ddot{X}_V\} + [C_V]\{\dot{X}_V\} + [K_V]\{X_V\} = \{F_V\}, \tag{1}$$

where $[M_V]$, $[C_V]$ and $[K_V]$ are, respectively, the mass, damping and stiffness matrices of the vehicle, details of which are described in Ref. [19]; $\{X_V\}$, $\{\dot{X}_V\}$ and $\{\ddot{X}_V\}$ are, respectively, the displacement, velocity and acceleration vectors of the vehicle, with

$$\{X_V\} = \{X_{V1}, X_{V2}, \ldots, X_{Vn}\}, \tag{2a}$$

$$\{X_{Vi}\} = \{Y_{1,i}, Z_{1,i}, R_{X1,i}, R_{Y1,i}, R_{Z1,i}, Y_{2,i}, Z_{2,i}, R_{X2,i}, R_{Y2,i}, R_{Z2,i}, Y_{3,i}, Z_{3,i}, R_{X3,i}, R_{Y3,i}, R_{Z3,i}\} \tag{2b}$$

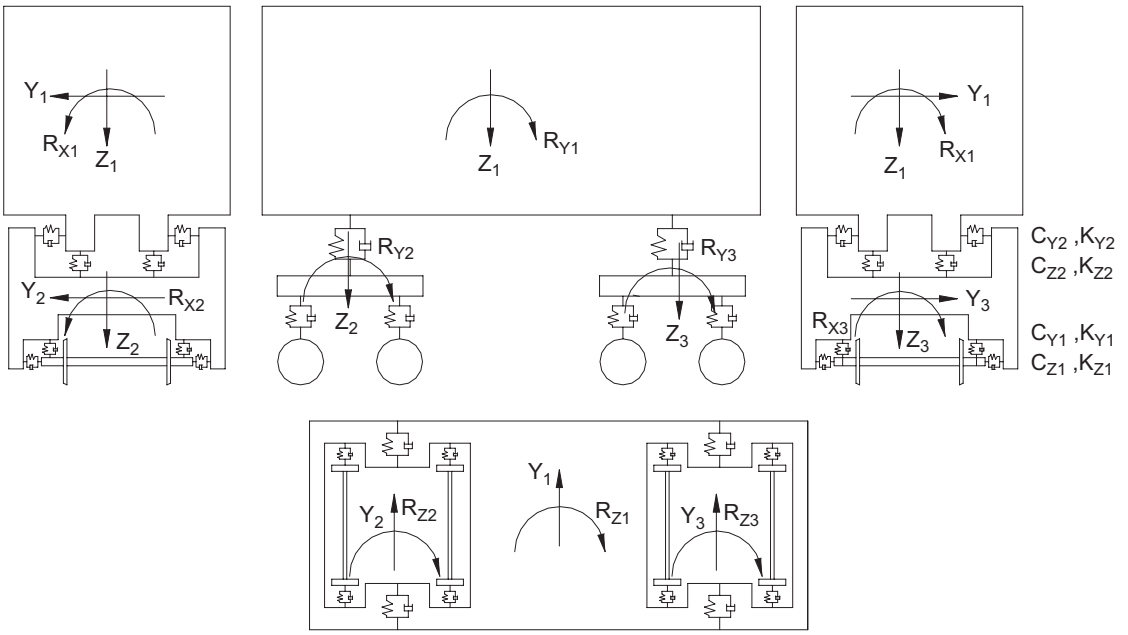

Fig. 1. Vehicle model for a 4-axle vehicle element.

and $\{F_V\}$ is the vector of forces transmitted from the wheel-sets to the bogies through the first suspension system, expressed as

$$\{F_V\} = \{F_{V1}, F_{V2}, \ldots, F_{Vn}\}, \tag{3a}$$

$$\{F_{V,}\} = \{F_{Y1,i}, F_{Z1,i}, F_{RX1,i}, F_{RY1,i}F_{RZ1,i}, F_{Y2,i}, F_{Z2,i}, F_{RX2,i}, F_{RY2,i}, F_{RZ2,i}, F_{Y3,i}, F_{Z3,i}, F_{RX3,i}, F_{RY3,i}, F_{RZ3,i}\}, \tag{3b}$$

where n is the number of vehicle. Detail informations are described in Section 2.3.

2.2. Bridge subsystem model

The bridge subsystem model is established by the finite element method, where the structural information for the bridge system can be expressed in 2 ways: the direct stiffness method [4,5,15–17,19] and the modal superposition method [4,13].

The modal superposition method is usually used for bridges with long span or low stiffness. Generally only a few modes are required to express the global deformation and the local deformation of the structural elements supporting the track, thus the dofs of the bridge model can be greatly reduced. The direct stiffness method is fit for the bridges with short span or high stiffness, or the local deflections and stress of certain members are concerned. When using the direct stiffness method, the bridge model can be established just by introducing the global mass, damping and stiffness matrices of the bridge system, including its superstructures, substructures, foundations and surrounding soils if needed. It is suitable for any bridge analysis whose scale of matrices and computational duration is acceptable. The bridge model in this paper is established based on the direct stiffness method.

When the bridge carries a railway, the track is laid on the bridge deck and the forces from the wheels of the train vehicle transmit to the bridge deck through the track. It is assumed that there is no relative displacement between the track and the bridge deck. The elastic effects of the track are also neglected. When the bridge is modeled spatially by finite element method, the motion equations of the bridge system can be expressed as

$$[M_B]\{\ddot{X}_B\} + [C_B]\{\dot{X}_B\} + [K_B]\{X_B\} = \{F_B\}, \tag{4}$$

where $[M_B]$, $[C_B]$ and $[K_B]$ are, respectively, the global mass, damping and stiffness matrices of the bridge; $\{X_B\}$, $\{\dot{X}_B\}$ and $\{\ddot{X}_B\}$ are, respectively, the displacement, velocity and acceleration vectors of the bridge system; $\{F_B\}$ is the vector of forces from the wheel-sets of the train on the bridge deck through the track, see Section 2.3.

The damping matrix in Eq. (4) is the Rayleigh damping expressed by the linear combination of mass matrix and stiffness matrix

$$[C] = \alpha[M] + \beta[K], \tag{5a}$$

$$\alpha = 4\pi \frac{\xi_1 f_1 f_2^2 - \xi_2 f_1^2 f_2}{f_2^2 - f_1^2}, \tag{5b}$$

$$\beta = \frac{1}{\pi} \frac{\xi_2 f_2 - \xi_1 f_1}{f_2^2 - f_1^2}, \tag{5c}$$

where f_1 and f_2 are the first- and second-order frequencies, and ξ_1 and ξ_2 are the first and second-order damping ratios of the bridge, respectively.

2.3. Wheel–rail interaction model

The modeling of wheel–rail interaction is a key in vehicle–bridge interaction system analysis. One type of wheel–rail interaction model is based on the force corresponding relationship [1,18,20], in which the tangent wheel–rail force is defined by the Kalker creep theory and the Shen's theory from the relative velocities of the vehicle subsystem and the bridge subsystem, while the normal wheel–rail force is defined by the Hertz contact theory from the relative displacement of the two subsystems. Despite of its accurate mechanics concept, this type of model has the following shortcomings:

(1) The curvature radii for both wheel and track at the contact point are required in using the Kalker creep theory, thus a time-consuming scanning calculation is inevitable in the wheel–rail contact geometry analysis.
(2) The relationship between the normal relative movement and the normal interaction force is nonlinear, which may cause difficulty in history integral calculation.
(3) The wheel–track seceding state is considered in the model, which may influence the convergence in the iteration procedures between the vehicle subsystem and the bridge subsystem. While generally speaking, the wheel–track secession in very short time has little engineering sense.

Another type of wheel–rail interaction model is based on the displacement corresponding relationship [4,5,19], in which the relative movement between the wheel and the bridge obeys a given assumption. This model can avoid the above shortcomings and is adopted in this paper.

The movement of a wheel-set is the function of the bridge deck movement, the track irregularity and the hunting movement of wheel-set, which can be expressed as

$$\mathbf{D}_W = \begin{Bmatrix} Y_W \\ Z_W \\ R_{XW} \end{Bmatrix} = \begin{Bmatrix} Y_D \\ Z_D \\ R_{XD} \end{Bmatrix} + \begin{Bmatrix} Y_I \\ Z_I \\ R_{XI} \end{Bmatrix} + \begin{Bmatrix} Y_H \\ 0 \\ 0 \end{Bmatrix}, \tag{6}$$

where $\mathbf{D}_W$ is displacement vector of wheel-set; Y, Z and R_X are, respectively, the lateral, vertical and rotational movements of the bridge deck cross-section; subscript W stands for the wheel displacement; subscript D stands for the bridge displacement at the center of the deck; subscript I stands for irregularity additional displacement defined in Section 2.4; Y_H is the wheel hunting movement. The velocity vector $\mathbf{V}_W$ and the acceleration vector $\mathbf{A}_W$ of the wheel-set can be defined in a similar way.

(4) The hunting movement between wheel-set and track is defined by

$$Y_H(X) = A_h \sin\left(\frac{2\pi X}{L_h} + \phi\right), \tag{7}$$

where X is the position coordinate of wheel-set along the track on the bridge; A_h, L_h and ϕ are, respectively, the hunting wavelength, amplitude and random phase angle of a certain wheel-set.

Thus, the forces on the vehicle subsystem and the bridge subsystem can be fully expressed.

Firstly, the effect of an individual wheel-set is studied, by assuming that the vehicle and bridge force vectors due to the ith wheel-set are $\tilde{\mathbf{F}}_{V,i}$ and $\tilde{\mathbf{F}}_{B,i}$, which are shortened as $\tilde{\mathbf{F}}_V$ and $\tilde{\mathbf{F}}_B$ in this section, respectively.

The vehicle subsystem force vector $\tilde{\mathbf{F}}_V$ consists of the forces from the first suspension system, which acts on the vehicle bogies. The bridge subsystem force vector $\tilde{\mathbf{F}}_B$ consists of the forces between wheel and track, which acts on the bridge deck. The vectors are defined as

$$\tilde{\mathbf{F}}_V = \{ F_{VY} \quad F_{VZ} \quad F_{VRX} \quad F_{VRY} \quad F_{VRZ} \}^{\mathrm{T}}, \tag{8a}$$

$$\tilde{\mathbf{F}}_B = \{ F_{BY} \quad F_{BZL} \quad F_{BZR} \}^{\mathrm{T}}, \tag{8b}$$

where F_{Vi} are the forces acting on the bogie in direction i; F_{BY} is the force acting on the bridge in direction Y at the position of the rail elevation; F_{BZL} and F_{BZR} are the forces acting on the bridge in direction Z at the left and right tracks, respectively.

The forces of the first suspension system consist of the spring force and the damping force, which are the functions of relative displacements and velocities between bogies and wheel-sets, respectively. The force between wheel and track is the sum of the spring and damping forces in the first suspension system, the static vehicle load and the inertial force of wheel-set. The static vehicle load is a constant value for a given vehicle, and the inertial force is the product of wheel-set mass and wheel-set acceleration. Thus the general force vector $\tilde{\mathbf{F}}$ can be expressed as

$$\tilde{\mathbf{F}} = \begin{Bmatrix} \tilde{\mathbf{F}}_V \\ \tilde{\mathbf{F}}_B \end{Bmatrix} == \begin{Bmatrix} \mathbf{F}_{KV} + \mathbf{F}_{CV} \\ \mathbf{F}_{KB} + \mathbf{F}_{CB} + \mathbf{F}_{MB} + \mathbf{F}_G \end{Bmatrix} = \mathbf{T} \begin{Bmatrix} \mathbf{D}_J \\ \mathbf{D}_W \\ \mathbf{V}_J \\ \mathbf{V}_W \\ \mathbf{A}_W \end{Bmatrix} + \begin{Bmatrix} 0 \\ \mathbf{F}_G \end{Bmatrix} = \mathbf{TU} + \begin{Bmatrix} 0 \\ \mathbf{F}_G \end{Bmatrix}, \tag{9}$$

where $\mathbf{F}_{KV}$ and $\mathbf{F}_{CV}$ are the spring and damping force vectors of the first suspension system acting on the vehicle element, respectively; $\mathbf{F}_{KB}$ and $\mathbf{F}_{CB}$ are the spring and damping force vectors of the first suspension system acting on the bridge, respectively; $\mathbf{F}_{MB}$ is the inertia force vector of wheel-set; $\mathbf{F}_G$ is static vehicle load vector of vehicle element; $\mathbf{D}_J$ and $\mathbf{V}_J$ are the displacement and velocity vectors of bogie, respectively; $\mathbf{F}_G$, $\mathbf{D}_J$ and $\mathbf{V}_J$ are defined in Eqs. (10a)–(10c) as

$$\mathbf{F}_G = \frac{1}{2} \{ 0 \quad F_{GZ} \quad F_{GZ} \}^{\mathrm{T}}, \tag{10a}$$

$$\mathbf{D}_J = \{ Y_J \quad Z_J \quad R_{XJ} \quad R_{YJ} \quad R_{ZJ} \}^{\mathrm{T}}, \tag{10b}$$

$$\mathbf{V}_J = \left\{ \dot{Y}_J \quad \dot{Z}_J \quad \dot{R}_{XJ} \quad \dot{R}_{YJ} \quad \dot{R}_{ZJ} \right\}^{\mathrm{T}}, \tag{10c}$$

where F_{GZ} is the static weight for each vehicle axle and subscript J stands for bogie.

The general movement vector $\mathbf{U}$ in Eq. (9) contains all system movement information needed for the system force vectors $\mathbf{F}_A$ and $\mathbf{F}_B$. Vectors $\mathbf{D}_W$, $\mathbf{V}_W$ and $\mathbf{A}_W$ can be obtained by Eq. (6) according to the bridge displacement, velocity and acceleration and the track irregularities at the position of the wheel.

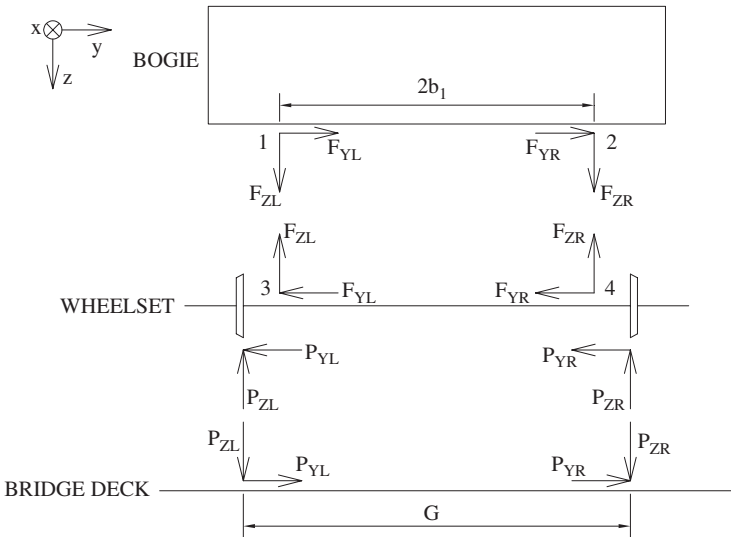

Fig. 2. Interaction forces of vehicle–bridge system.

Fig. 2 shows the interaction forces between the bogie and the wheel and between the wheel and the bridge deck, from which Matrix **T** in Eq. (9), an 8 × 19 transformation matrix between vector $\tilde{\mathbf{F}}$ and vector **U**, can be derived as follows:

(1) As shown in Fig. 2, the lateral and vertical forces at the left side and right side of the first suspension system are

$$\begin{cases} F_{YL} = K_{Y1}(Y_3 - Y_1) + C_{Y1}(\dot{Y}_3 - \dot{Y}_1), \\ F_{YR} = K_{Y1}(Y_4 - Y_2) + C_{Y1}(\dot{Y}_4 - \dot{Y}_2), \\ F_{ZL} = K_{Z1}(Z_3 - Z_1) + C_{Z1}(\dot{Z}_3 - \dot{Z}_1), \\ F_{ZR} = K_{Z1}(Z_4 - Z_2) + C_{Z1}(\dot{Z}_4 - \dot{Z}_2), \end{cases} \tag{11}$$

where F_{YL} and F_{YR} are lateral forces at the left side and right side, and F_{ZL} and F_{ZR} are vertical forces at the left side and right side of the first suspension system, respectively; Y_k and Z_k and their derivatives are the displacements and velocities in directions Y and Z for point k ($k = 1, 2, 3, 4$) in Fig. 2, K_{Y1} and K_{Z1} are the lateral and vertical spring coefficients, and C_{Y1} and C_{Z1} are the damping coefficients in the first suspension system, respectively.

The lateral and vertical displacements of Points 1, 2, 3 and 4 are

$$\begin{cases} Y_1 = Y_2 = Y_J + sR_{ZJ} - h_3R_{XJ}, \\ Y_3 = Y_4 = Y_W, \\ Z_{1,2} = Z_J - sR_{YJ} \mp b_1R_{XJ}, \\ Z_{3,4} = Z_W \mp b_1R_{XW}, \end{cases} \tag{12}$$

where s is the longitudinal distance between the gravity centers of car body and bogies, with $s>0$ for the front bogie and $s<0$ for the rear one; h_3 is the vertical distance between the gravity center of bogie and the upper suspension point of the first suspension system; b_1 is the half-lateral distance between left and right components in the first suspension system. The lateral and vertical velocities of Points 1, 2, 3 and 4 are can be defined in a similar form with Eq. (12).

The force equilibrium conditions of wheel-set are

$$\begin{cases} F_{YL}+F_{YR}+P_{YL}+P_{YR}=0, \\ F_{ZL}+F_{ZR}+P_{ZL}+P_{ZR}=0, \\ (F_{ZL}-F_{ZR})b_1+(P_{ZL}-P_{ZR})\frac{G}{2}+(P_{YL}+P_{YR})R_W=0, \end{cases} \tag{13}$$

where G is the horizontal distance between left and right rails and R_W the radius of the wheel. The global forces acting on the bogie are

$$\begin{cases} F_{AY}=F_{YL}+F_{YR}, \\ F_{AZ}=F_{ZL}+F_{ZR}, \\ F_{ARX}=b_1(F_{ZR}-F_{ZL})-h_3(F_{YL}+F_{YR}), \\ F_{ARY}=-s(F_{ZL}+F_{ZR}), \\ F_{ARZ}=s(F_{YL}+F_{YR}). \end{cases} \tag{14}$$

The global forces acting on the bridge are

$$\begin{cases} F_{BY}=P_Y+m_0\ddot{Y}_W, \\ F_{BZL}=P_{ZL}+\frac{1}{2}m_0\ddot{Z}_W-\frac{I_{X0}\ddot{R}_{XW}}{G}, \\ F_{BZR}=P_{ZR}+\frac{1}{2}m_0\ddot{Z}_W+\frac{I_{X0}\ddot{R}_{XW}}{G}, \end{cases} \tag{15}$$

where m_0 is the mass, and I_{X0} the moment of inertia about direction X of the wheel-set.

Thus matrix $\mathbf{T}$ can be obtained by solving the simultaneous equations from Eqs. (10) to (14) as

$$\mathbf{T}=\begin{bmatrix} \mathbf{K}_{JV} & \mathbf{K}_{WV} & \mathbf{C}_{JV} & \mathbf{C}_{WV} & 0 \\ \mathbf{K}_{JB} & \mathbf{K}_{WB} & \mathbf{C}_{JB} & \mathbf{C}_{WB} & \mathbf{M}_{WB} \end{bmatrix}, \tag{16a}$$

$$\mathbf{K}_{JV}=\begin{bmatrix} -2K_{Y1} & 0 & 2h_3K_{Y1} & 0 & -2sK_{Y1} \\ 0 & -2K_{Z1} & 0 & 2sK_{Z1} & 0 \\ 2h_3K_{Y1} & 0 & -2b_1^2K_{Z1}-2h_3^2K_{Y1} & 0 & 2sh_3K_{Y1} \\ 0 & 2sK_{Z1} & 0 & -2s^2K_{Z1} & 0 \\ -2sK_{Y1} & 0 & 2sh_3K_{Y1} & 0 & -2s^2K_{Y1} \end{bmatrix}, \tag{16b}$$

$$\mathbf{K}_{JB}=\begin{bmatrix} 2K_{Y1} & 0 & -2h_3K_{Y1} & 0 & 2sK_{Y1} \\ -2K_{Y1}R_W/G & K_{Z1} & 2(-b_1^2K_{Z1}+h_3R_WK_{Y1})/G & -sK_{Z1} & -2sK_{Y1}R_W/G \\ 2K_{Y1}R_W/G & K_{Z1} & -2(-b_1^2K_{Z1}+h_3R_WK_{Y1})/G & -sK_{Z1} & 2sK_{Y1}R_W/G \end{bmatrix}, \tag{16c}$$

$$\mathbf{K}_{WV}=\begin{bmatrix} 2K_{Y1} & 0 & 0 \\ 0 & 2K_{Z1} & 0 \\ -2h_3K_{Y1} & 0 & 2b_1^2K_{Z1} \\ 0 & -2sK_{Z1} & 0 \\ 2sK_{Y1} & 0 & 0 \end{bmatrix}, \tag{16d}$$

$$\mathbf{K}_{WB}=\begin{bmatrix}-2K_{Y1} & 0 & 0\\ 2K_{Y1}R_W/G & -K_{Z1} & 2b_1^2K_{Z1}/G\\ -2K_{Y1}R_W/G & -K_{Z1} & -2b_1^2K_{Z1}/G\end{bmatrix}, \tag{16e}$$

$$\mathbf{M}_{WB}=\begin{bmatrix}m_0 & 0 & 0\\ 0 & m_0/2 & -I_{X0}/G\\ 0 & m_0/2_0 & I_{X0}/G\end{bmatrix}. \tag{16f}$$

The sub-matrices $\mathbf{C}_{JV}$, $\mathbf{C}_{JB}$, $\mathbf{C}_{WV}$ and $\mathbf{C}_{WB}$ have the similar forms with $\mathbf{K}_{JV}$, $\mathbf{K}_{JB}$, $\mathbf{K}_{WV}$ and $\mathbf{K}_{WB}$, just by changing spring coefficients K_{Y1} and K_{Z1} into damping coefficients C_{Y1} and C_{Z1}, respectively. All the coefficients in matrix $\mathbf{T}$ are known and constant values, so it can be calculated before the history integral calculation.

Since the input movement vector in Eq. (6) and output force vector in Eq. (9) for bridge system are about the mid point between the two rails of a track (assumed as Point D), while the relative values in Eq. (4) are about the gravity center of bridge cross-section (assumed as Point C), the following transformation relationships should be used:

$$\begin{Bmatrix}Y_D\\ Z_D\\ R_{XD}\end{Bmatrix}=\begin{Bmatrix}Y_C-R_{XC}d_Z\\ Z_C+R_{XC}d_Y\\ R_{XC}\end{Bmatrix}, \tag{17a}$$

$$\begin{Bmatrix}F_{CY}\\ F_{CZ}\\ F_{CRX}\end{Bmatrix}=\begin{bmatrix}1 & 0 & 0\\ 0 & 1 & 1\\ -d_Z & d_Y-\dfrac{G}{2} & d_Y+\dfrac{G}{2}\end{bmatrix}\begin{Bmatrix}F_{BY}\\ F_{BZL}\\ F_{BZR}\end{Bmatrix}, \tag{17b}$$

where subscripts D and C stand for Points D and C; d_Y and d_Z are horizontal and vertical distances between C and D, respectively.

Thus, the vehicle force vector $\mathbf{F}_V$ in Eq. (1) and the bridge force vector $\mathbf{F}_B$ in Eq. (4) can be obtained by summing the force vectors of all wheel-sets

$$\begin{cases}\mathbf{F}_V=\sum_{i=1}^{N_W}\mathbf{T}_{JV}\tilde{\mathbf{F}}_{V,i},\\ F_B=\sum_{i=1}^{N_W}\mathbf{T}_{CB}\tilde{\mathbf{F}}_{B,i},\end{cases} \tag{18}$$

where $\mathbf{T}_{JV}$ is the transfer matrix from $\tilde{\mathbf{F}}_{V,i}$ to $\tilde{\mathbf{F}}_V$, and $\mathbf{T}_{CB}$ is the transfer matrix from $\tilde{\mathbf{F}}_{B,i}$ to $\tilde{\mathbf{F}}_B$, which are defined as

$$t_{JV,i,j}=\begin{cases}1, & i=m_k,j=k,k=1,\ldots,5,\\ 0 & \text{others.}\end{cases} \tag{19}$$

$$t_{CB,i,j}=\begin{cases}\dfrac{d_2}{d_1+d_2}, & i=n_{1k},j=k,k=1,\ldots,3,\\ \dfrac{d_1}{d_1+d_2}, & i=n_{2k},j=k,k=1,\ldots,3,\\ 0 & \text{others,}\end{cases} \tag{20}$$

where $t_{JV,i,j}$ and $t_{CB,i,j}$ are the elements of the ith row and jth column in the transformation matrices $\mathbf{T}_{JV}$ and $\mathbf{T}_{CB}$, respectively; m_1, m_2, m_3, m_4 and m_5 are the vehicle subsystem dof numbers of the bogie linked to the related wheel-set in directions Y, Z, R_X, R_Y and R_Z, respectively; d_1 and d_2 are the distances between the wheel

position and the neighboring bridge nodes N_1 and N_2 in both sides, respectively; n_{11}, n_{12} and n_{13} are dof numbers of bridge subsystem at N_1 in directions Y, Z and R_X, while n_{21}, n_{22} and n_{23} are those at N_2 in directions Y, Z and R_X, respectively.

2.4. Additional movement of track irregularity and hunting

The track irregularity reflects the relative position between bridge deck and rails, and the hunting movement reflects relative position between rails and wheel-set, thus the relative position of bridge and wheel-set can be expressed by the algebraic sum of track irregularity and hunting movement, shown in Eq. (6).

The additional track irregularity displacements Y_I, Z_I and R_{XI} of wheel-set at its gravity center can be expressed as

$$\begin{Bmatrix} Y_I \\ Z_I \\ R_{XI} \end{Bmatrix} = \begin{Bmatrix} \frac{1}{2}(Y_{IL} + Y_{IR}) \\ \frac{1}{2}(Z_{IL} + Z_{IR}) \\ \frac{1}{G}(-Z_{IL} + Z_{IR}) \end{Bmatrix}, \tag{21}$$

where Y_{IL} and Y_{IR} are irregularities of left and right rails in direction Y, while Z_{IL} and Z_{IR} are those in direction Z, respectively.

The additional hunting movement displacements between wheel-set and track can be found in Eq. (7).

The track irregularity and hunting movement also cause additional velocity of wheel-set relative to bridge deck, which can be expressed in a differential form

$$\dot{E} = \lim_{\Delta t \to 0} \frac{\Delta E}{\Delta t} = \lim_{\Delta t \to 0} \frac{\Delta E}{\Delta X / V} = V \lim_{\Delta t \to 0} \frac{\Delta E}{\Delta X} = V \frac{\partial E}{\partial X}, \tag{22}$$

where E stands for bridge-wheel relative displacement Y_{IL}, Y_{IR}, Z_{IL}, Z_{IR} or Y_H, correspondingly; V is the train speed.

The additional acceleration of the track irregularity and hunting movement can be derived in similar method as

$$\ddot{E} = \lim_{\Delta t \to 0} \frac{\Delta \dot{E}}{\Delta t} = \lim_{\Delta t \to 0} \frac{\Delta \dot{E}}{\Delta X / V} = V \lim_{\Delta t \to 0} \frac{\Delta \dot{E}}{\Delta X} = V \frac{\partial \dot{E}}{\partial X} = V^2 \frac{\partial E}{\partial X}. \tag{23}$$

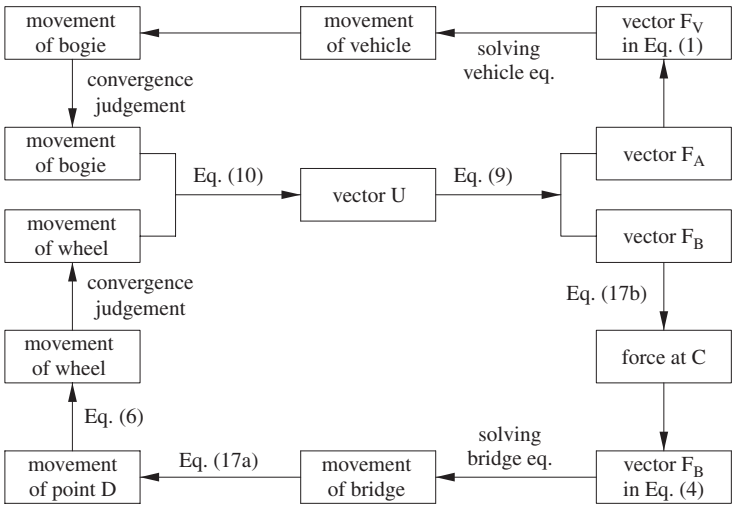

Fig. 3. Iterative calculation steps.

2.5. History integral

The simultaneous differential equations of Eqs. (1) and (4) are solved by numerical integral method, and the displacement corresponding relationship between the bridge system and vehicle system can be determined by iterative calculations shown in Fig. 3.

The iterative calculation is not an unconditional convergence process, because the forces and movements of the vehicle subsystem and the bridge subsystem need to be transferred and solved separately, thus the step of history integral and the convergent errors for both subsystems can only be determined through trial. Generally, an integral step of 10^{-4} s and a convergent error of 1/1000 for both subsystems are accuracy-acceptable in most dynamic analyses of railway bridges.

3. Case study

3.1. Information of the train

The case study concerns the Pioneer Train passing on the Gouhe Bridge in QSSPR. The Pioneer Train consists of 6 passenger cars, with the 1st, 3rd, 4th and 6th cars being tractors, and the 2nd and 5th cars trailers. The average static axle loads for tractors and trailers are 144.2 and 134.9 kN, respectively. Both the tractor and trailer cars are 25.5 m in length. The design speed of the Pioneer Train is 220 km/h and the maximum speed reached 270 km/h in the experiment. Fig. 4 shows the dimensions of the first three cars of the Pioneer Train. The calculation train speeds in the vehicle–bridge interaction analysis are 150, 170, 190, 210, 230, 250 and 270 km/h, respectively.

3.2. Information of the bridge

The Gouhe Bridge consists of 28 successive simply supported double bound PC girders with 24 m-span lengths and box sections, which are one of the most common types in the bridges of QSSPR. The view of the bridge and the cross-section of the girder are shown in Figs 5 and 6, respectively. The bridge deck is mounted with ballastless PC slab tracks, shown in Fig. 9. The substructures of the bridge are rounded end piers with friction piles, end-bearing piles and open-cut foundations.

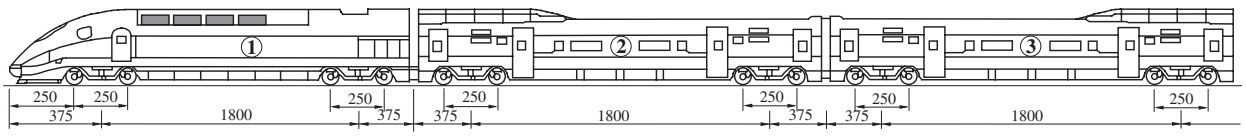

Fig. 4. Composition of the Pioneer train.

Fig. 5. View of the Gouhe River Bridge.

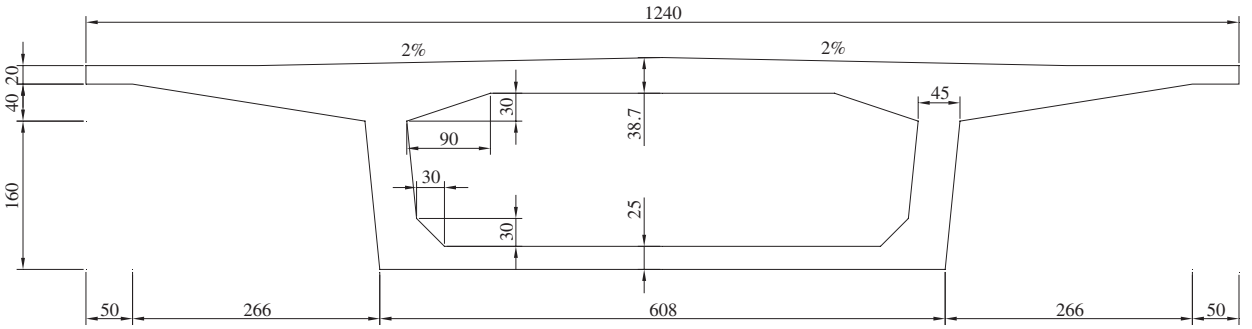

Fig. 6. Cross-section of the 24 m-span beam (unit: cm).

Table 1
Natural frequencies of the girder (Hz^{-1})

Item	Vertical	Torsional	Lateral
Calculation	7.57	11.73	19.39
Measurement	7.57	11.68	19.50

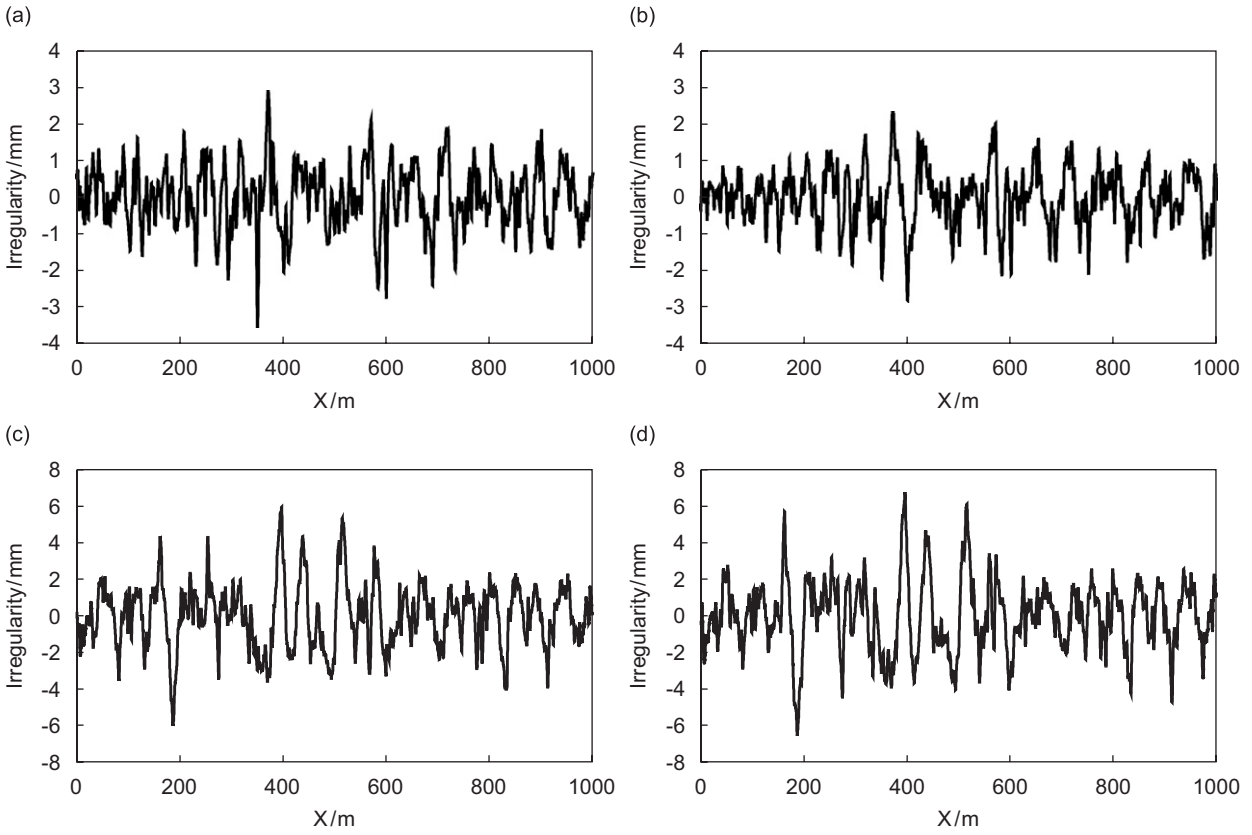

Fig. 7. Track irregularity curves measured in QSSPR.

The bridge segment from the 19–28th span is modeled. It is assumed that the bottoms of piers are fixed due to good geological condition and stiff foundations. The measured and the calculated natural frequencies of the bridge are listed in Table 1.

3.3. Information of track irregularity and hunting movement

The vertical and lateral irregularities for left and right rails of the track are taken into consideration by using the data measured in the QSSPR. The length of the data is 2500 m and the samples of 1000 m are plotted in Fig. 7. The maximum amplitudes of vertical and lateral irregularities are 8.59 and 3.84 mm.

The coefficients of hunting movement are taken as $L_h = 12$ m and $A_h = 5$ mm based on similar engineering cases [11].

3.4. Field experiment

To investigate the dynamic behaviors of the bridge under high-speed trains and to verify the analytical model, the field experiment on the bridge was carried out on September 2–11, 2002 [12], lasted for 10 days. The sensor locations were arranged at the end and the mid-span sections of the 22nd and the 23rd spans, and the tops of the 22nd and the 23rd piers, as shown in Fig. 8, where A, D, R and S indicate acceleration, displacement, rail force and concrete strain for measurement points in given directions, respectively. The accelerations and the lateral displacements of bridge mid-span were measured by sensors 891-4 mounted on the bridge deck, the vertical displacements were measured by LVDT sensors linked with the girder by steel chords, and the rail forces and concrete strains were measured by strain gauges. All the sensors and gauges were calibrated before and after the experiment. There were 24 groups of data measured in the experiment, with the train speed ranging from 5 to 270 km/h. The Pioneer Train running on the Gouhe Bridge during the experiment is shown in Fig. 9.

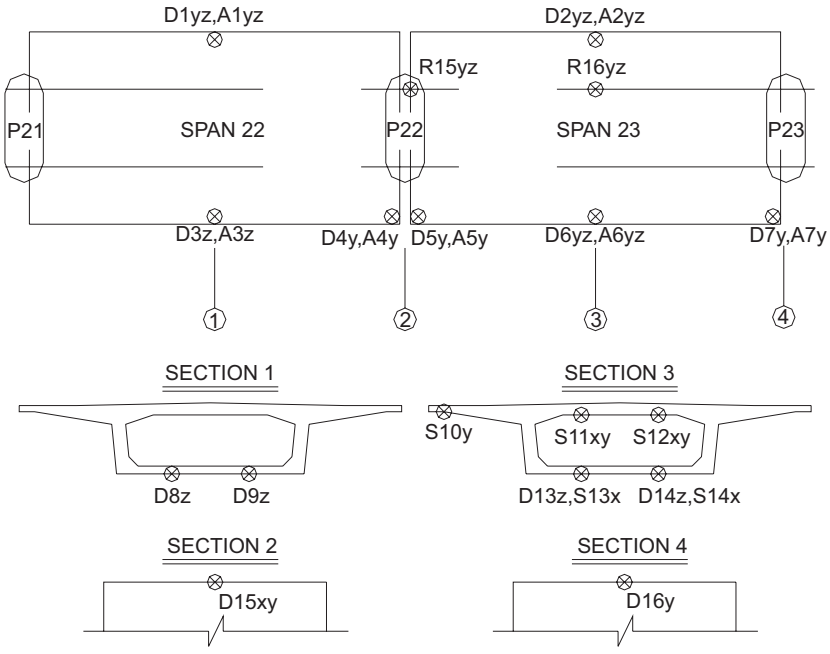

Fig. 8. Sensors arranged on the bridge.

Fig. 9. Pioneer Train running on the Gouhe Bridge.

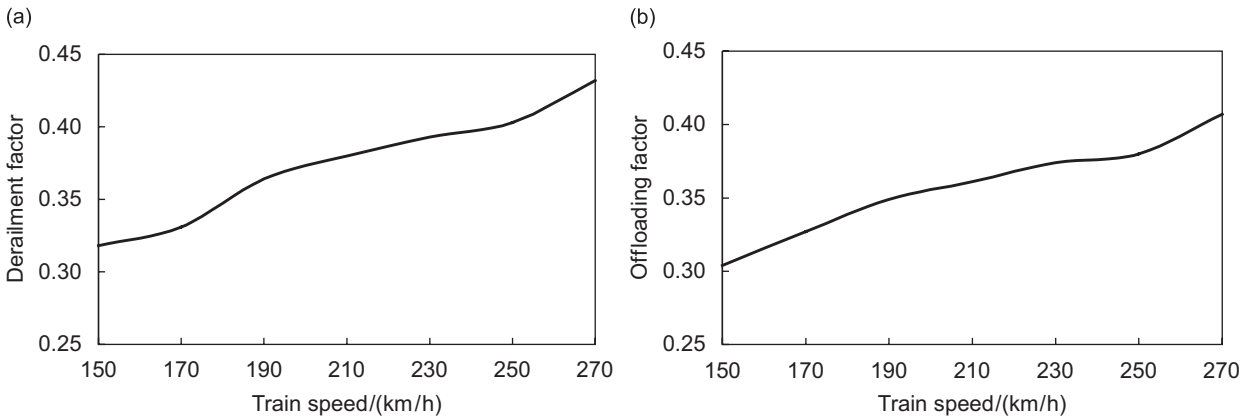

Fig. 10. Calculated vehicle derailment factors and offloads factors versus train speed.

3.5. *Vehicle responses*

The derailment factors offload factors and lateral wheel–rail forces are taken as the running safety indexes of vehicles. Their definitions and the corresponding allowances for high-speed trains in China are

$$\text{Derailment factor} = \max\left(\frac{Q_L}{P_L}, \frac{Q_R}{P_R}\right) \leqslant 0.8, \tag{24a}$$

$$\text{Offload factor} = \frac{|P_L - P_R|}{P_L + P_R} \leqslant 0.6, \tag{24b}$$

$$\text{Lateral wheel} - \text{rail force} = |Q_L + Q_R| \leqslant 0.85(F_{GZ}/3 + 10\,\text{kN}), \tag{24c}$$

where P_L and P_R are the vertical forces, Q_L and Q_R are the lateral forces for the left and right wheels of wheelset, respectively.

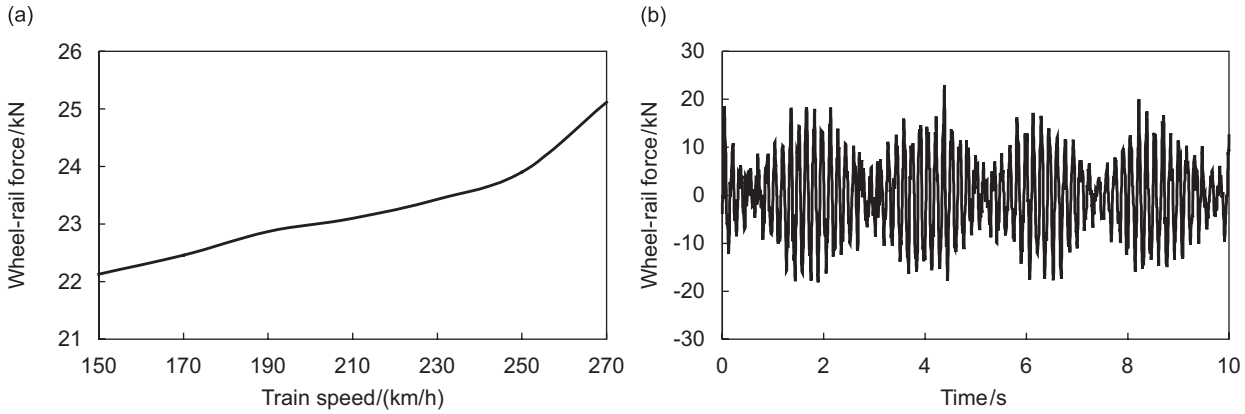

Fig. 11. Calculated lateral wheel–rail forces.

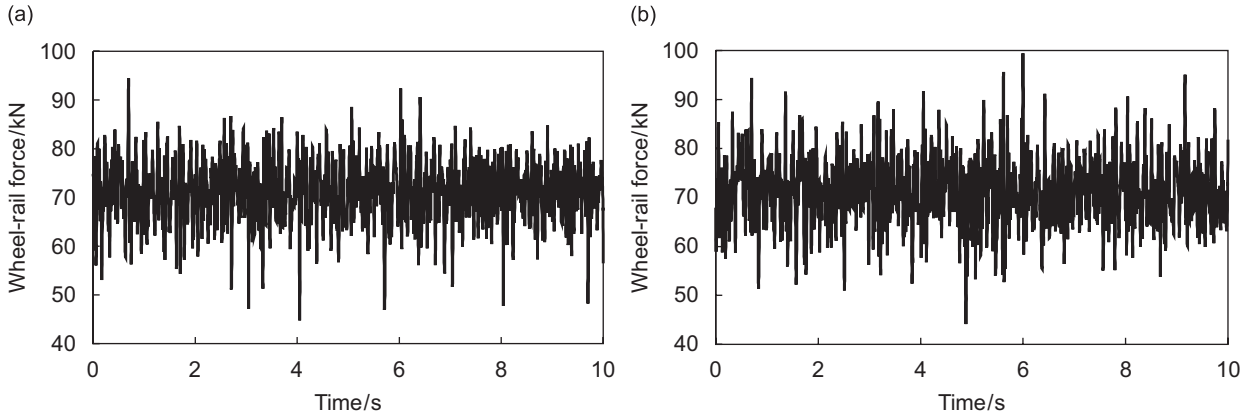

Fig. 12. Calculated vertical wheel–rail forces.

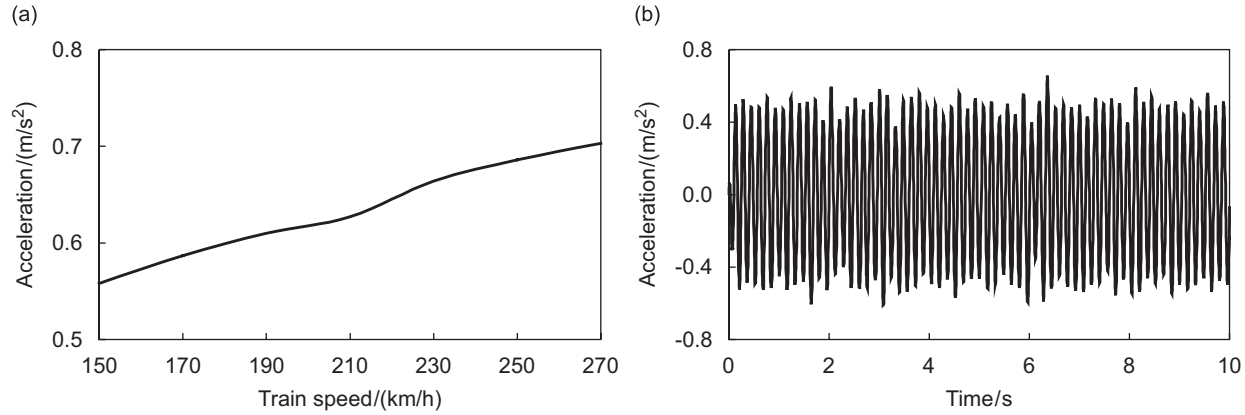

Fig. 13. Calculated lateral car-body acceleration.

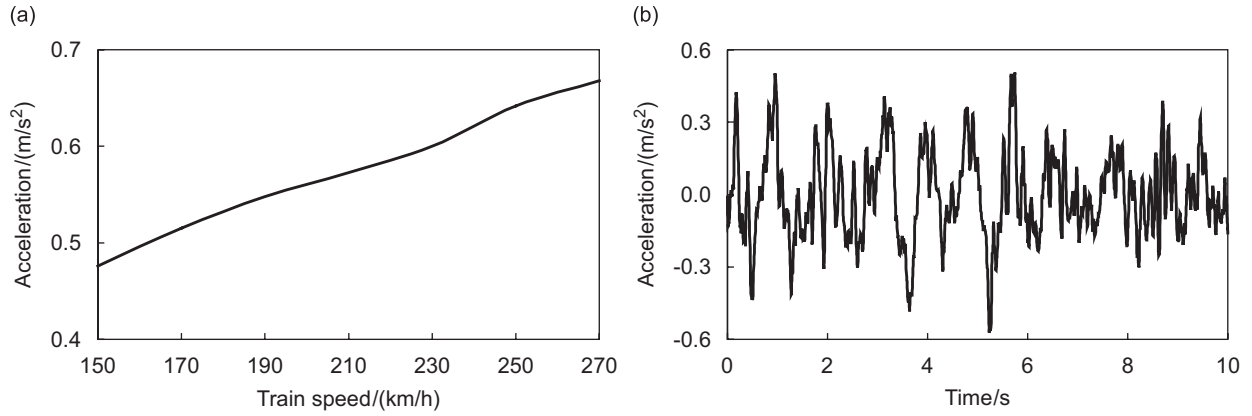

Fig. 14. Calculated vertical car body acceleration.

Table 2
Maximum responses of vehicles

Item		Tractor	Trailer	Allowance
Derailment factor Q/P		0.432	0.399	0.8
Offload factor $\Delta P/P$		0.407	0.358	0.6
Lateral wheel/rail force (kN^{-1})		25.12	24.44	Tractor: 49.4, Trailer: 46.7
Car-body acceleration (ms^{-2})	Vertical	0.703	0.651	1.0
	Lateral	0.688	0.667	1.3

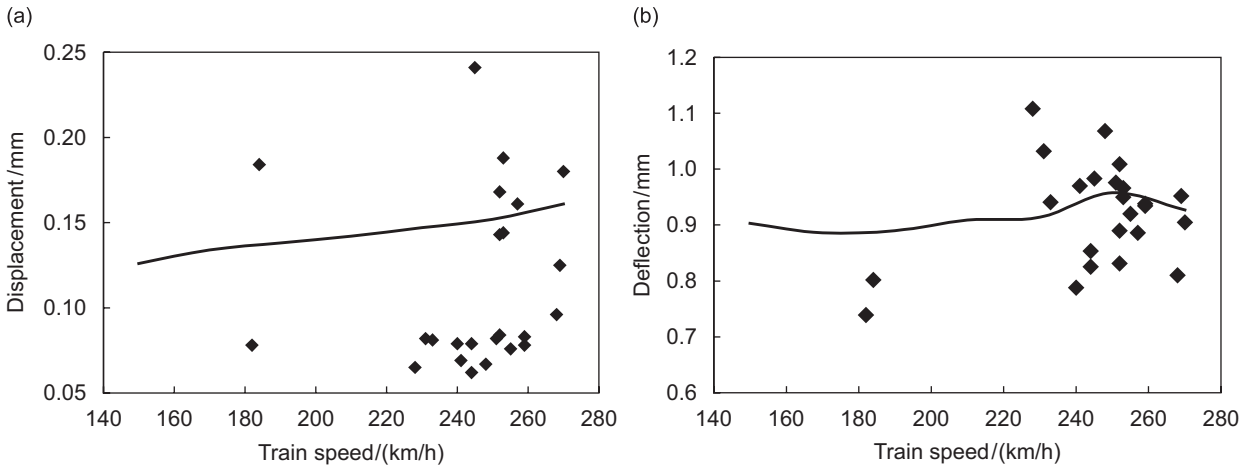

Fig. 15. Distribution of maximum girder displacement versus train speed.

The car-body accelerations in lateral and vertical directions are taken as the running stability indexes of vehicles, whose allowances are, respectively, 1.0 and 1.3 m/s^2 in the Chinese Code.

Shown in Figs. 10–14 are, respectively, the distributions of the safety indexes and the car-body accelerations of train vehicles versus train speed, and some typical response histories. It can be observed that the derailment factors, offload factors, lateral wheel–rail forces, lateral and vertical car-body accelerations of the Pioneer Train increase with the train speed and no obvious peak appeared within the train speed range of 150–270 km/h.

The followings are two important explanations about the calculated results:

(1) The wheel–rail forces were measured as well as calculated, but the two results represent different physical meanings. The measured result indicates the forces acting on the track at given position, while the calculated one the forces acting on certain wheel-set in the whole duration concerned.

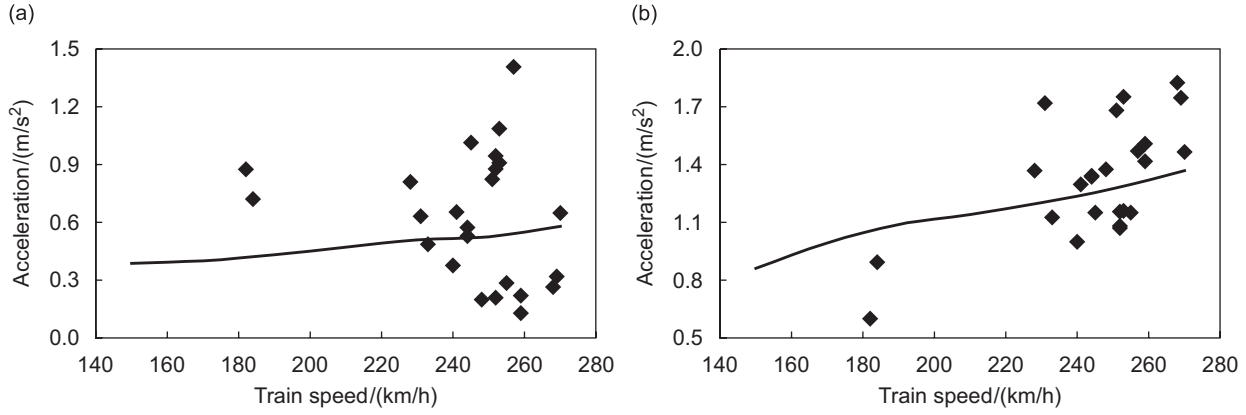

Fig. 16. Distribution of maximum girder acceleration versus train speed.

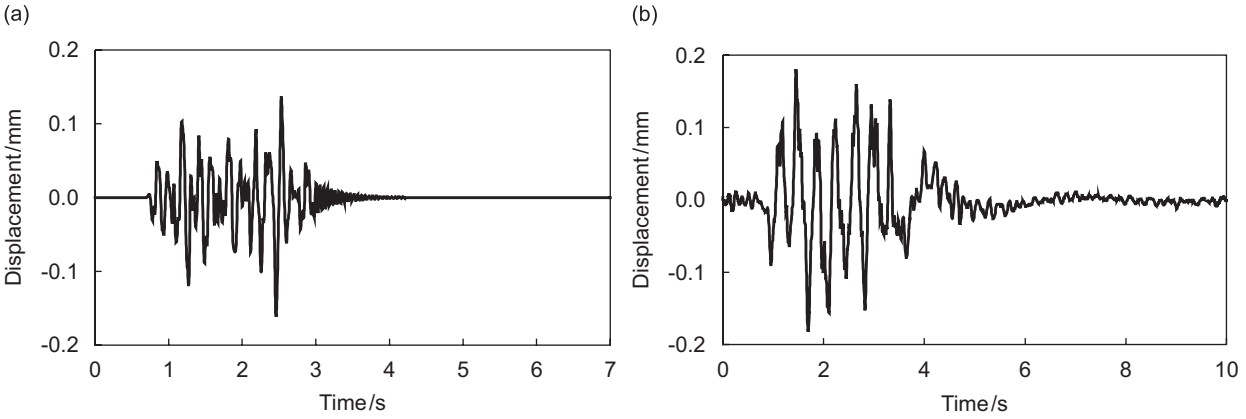

Fig. 17. Lateral displacement histories of girder at mid-span.

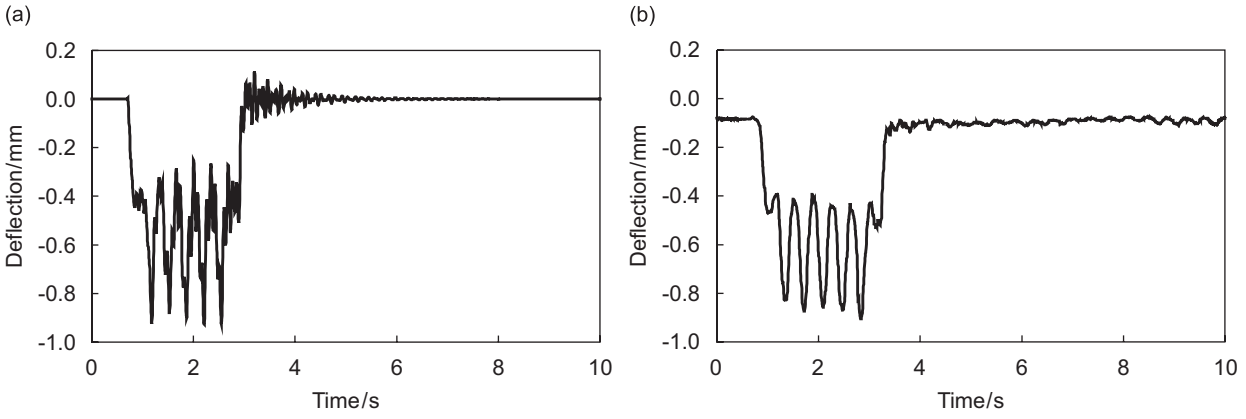

Fig. 18. Vertical deflection histories of girder at mid-span.

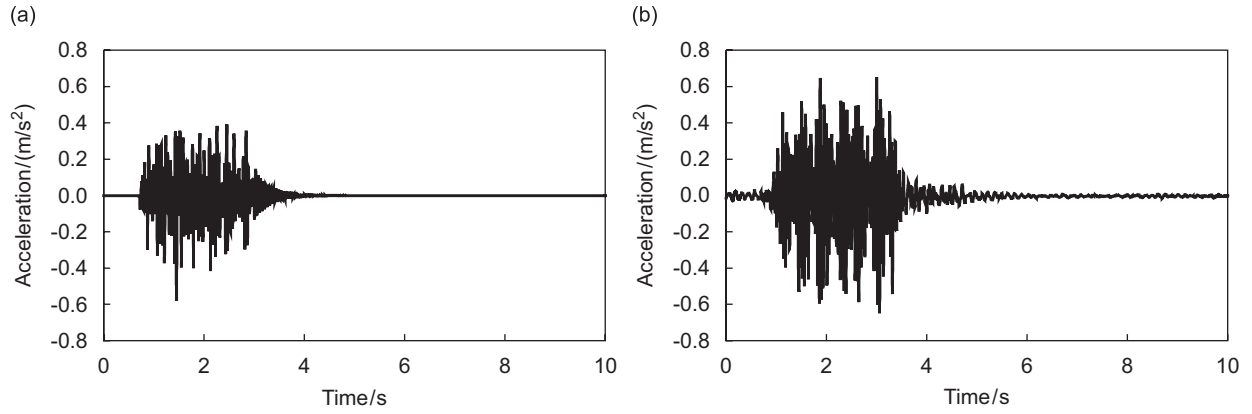

Fig. 19. Lateral acceleration histories of girder at mid-span.

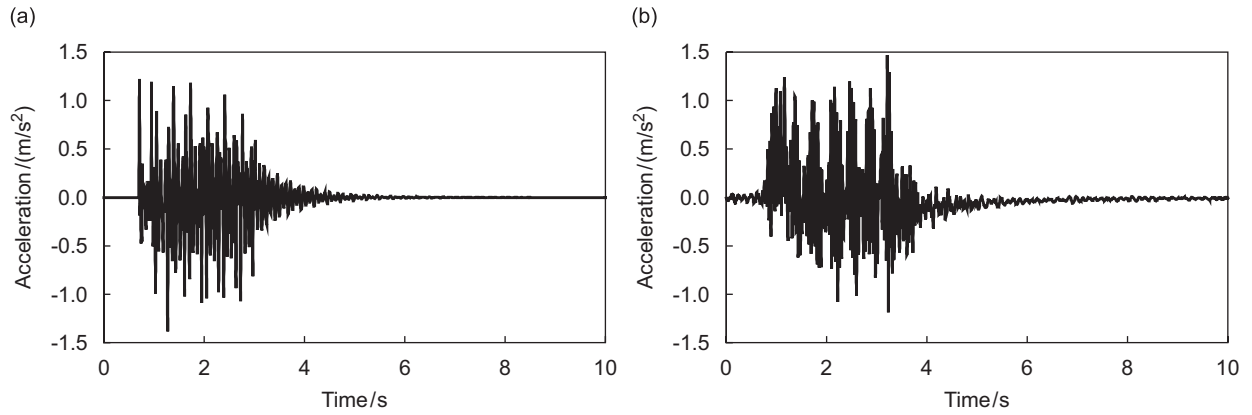

Fig. 20. Vertical acceleration histories of girder at mid-span.

Table 3
Maximum responses of bridge girder

Bridge response		Calculation	Measurement		
			Max	Mean	Standard deviation
Displacement (mm^{-1})	Lateral	0.161	0.241	0.112	0.051
	Vertical	0.958	1.108	0.920	0.091
Acceleration (ms^{-2})	Lateral	0.579	1.406	0.625	0.334
	Vertical	1.368	1.967	1.387	0.318

(2) It is assumed that the lateral wheel–rail force acts only on one side rail of the track at any moment, where a positive force stands for the force acting on the right rail and a negative one on the left.

The maximum responses of vehicles are listed in Table 2. It can be found that all the safety indexes fulfill the safety allowances.

3.6. Bridge responses

The lateral displacements, vertical deflections, lateral and vertical accelerations of the bridge at mid-span are studied. Shown in Figs. 15 and 16, respectively, are their distributions versus train speed for both calculated

and measured results, where the solid lines stand for calculated average results and the diamonds for measured data. The typical calculated and measured histories of bridge responses at train speed of 270 km/h are shown in Figs. 17–20.

Figs. 17–20 show that the measured results are rather scattering, it is partly due to the influences of the random factors such as the track irregularities, train wheel abnormalities, etc.

The Maximum calculated and measured responses of bridge girder are listed in Table 3. The results show that both the measured and calculated accelerations of Gouhe Bridge fulfill the allowance given by the Chinese Code for High-speed Railway Bridges, which are 1.40 and 3.50 m/s^2 for lateral and vertical accelerations, respectively.

4. Conclusions

The following conclusions can be summarized up from this paper:

(1) The dynamic analytical model of the vehicle–bridge system and the computer simulation method proposed in this paper can well reflect the vibration characteristics of the bridge and the high-speed train vehicles. The calculated results are well in accordance, both in response curves, in amplitudes and in distribution tendencies, with the experimental data, which verified the effectiveness of the analytical model and the computer simulation method.
(2) The 24 m-span PC box girders on QSSPR have perfect dynamic characteristics. Their lateral and vertical accelerations from both calculations and measurements fulfill the currently recognized safety and serviceability standards of high-speed railway bridges.
(3) The Pioneer Train has good running properties. In the speed range of 150–270 km/h, the derailment factors offload factors and lateral wheel–rail forces all fulfill the currently recognized running safety standards of high-speed trains.

Acknowledgments

This study is sponsored by the National Natural Science Foundation of China (Grant No. 50538010) and the Flander-China Bilateral Project of Belgium (BIL 04/17).

References

[1] Y.K. Cheung, F.T.K. Au, D.Y. Zheng, Y.S. Cheng, Vibration of multi-span bridges under moving vehicles and trains by using modified beam vibration functions, *Journal of Sound and Vibration* 228 (1999) 611–628.
[2] G. De Roeck, J. Maeck, A. Teughels, Train–bridge interaction: validation of numerical models by experiments on high-speed railway bridge in Antoing. *Proceedings of TIVC'2001*, Beijing, November 2001, pp. 283–294.
[3] G. Diana, F. Cheli, Dynamic interaction of railway systems with large bridges, *Vehicle System Dynamics* 18 (1989) 71–106.
[4] R.V. Dukkipati, *Vehicle Dynamics*, Alpha Science International Ltd., Pangourne, 2000.
[5] L. Frýba, *Vibration of Solids and Structures Under Moving Loads*, Thomas Telford, London, 1999.
[6] R. Gao, H. Xia, *Research on Dynamic Experiments of Bridges on Qin-Shen Special Passenger Railway*, Beijing Jiaotong University, Beijing, 2003 (in Chinese).
[7] M.F. Green, D. Cebon, Dynamic response of highway bridges to highway vehicle loads: theory and experimental validation, *Journal of Sound and Vibration* 170 (1994) 51–78.
[8] M. Klasztorny, Vertical vibration of a multi-span bridge under a train moving at high speed. *Proceedings of EURODYN'99*, Vol. 2, Rotterdam, 1999, pp. 651–656.
[9] J.W. Kwark, E.S. Choi, Y.J. Kim, B.S. Kim, S.I. Kim, Dynamic behavior of two-span continuous concrete bridges under moving high-speed train, *Computers & Structures* 82 (2004) 463–474.
[10] Z.Y. Shen, J.K. Hedrick, J.A. Elkins, A comparison of alternative creep force models for rail vehicle dynamic analysis. *Eighth IAVSD Symposium*, MIT, Cambridge, 1983, pp. 591–605.
[11] F.T. Wang, *Vehicle Dynamics*, China Railway Press, Beijing, 1994.
[12] H. Xia, N. Zhang, G. De Roeck, Dynamic analysis of high speed railway bridge under articulated trains, *Computers & Structures* 81 (2003) 2467–2478.
[13] H. Xia, N. Zhang, *Dynamic Interaction of Vehicles and Structures*, Science Press, Beijing, 2005 (in Chinese).

[14] Y.L. Xu, N. Zhang, H. Xia, Vibration of coupled train and cable stayed bridge system in cross wind, *Engineering Structures* 26 (2004) 1389–1406.
[15] Y.B. Yang, J.D. Yau, L.C. Hsu, Vibration of simple beams due to trains moving at high speed, *Journal of Engineering Structures* 19 (1997) 936–944.
[16] Y.B. Yang, J.D. Yau, *Vehicle–bridge Interaction Dynamics, with Application to High-Speed Railways*, World Scientific, Singapore, 2004.
[17] Y.B. Yang, J.D. Yau, Vehicle–bridge interaction element for dynamic analysis, *Journal of Structural Engineering—ASCE* 123 (1997) 1512–1518.
[18] W.M. Zhai, H. True, Vehicle–track dynamics on a ramp and on the bridges: simulation and measurements, *Vehicle System Dynamics (Supplement)* 33 (1999) 604–615.
[19] N. Zhang, H. Xia, *Study on Vehicle–bridges Interaction Simulation of Beijing-Shanghai High Speed Railway*, Beijing Jiaotong University, Beijing, 2005 (in Chinese).
[20] Q.L. Zhang, Q. Vrouwenvelder, J. Wardenier, Numerical simulation of train–bridge interactive dynamics, *Journal of Computers and Structures* 79 (2001) 1059–1075.